Unlocking the Potential of Battery Research

Unlocking the Potential of Battery Research: Advanced Characterization of Cell Components

PerkinElmer
For the Better

Wiley Analytical Science

A New Expert Insight.
Download for free.

Battery research is essential to meet the growing demand for reliable, efficient, cost-effective energy storage solutions.

This expert insight presents recent research on solid polymer electrolytes (SPEs), recycling methods for lithium-ion batteries (LIBs), and cathode degradation during extreme fast charging (XFC) of electric vehicles.

PerkinElmer®
For the Better

WILEY

RESEARCH ARTICLE

ADVANCED
ENERGY & SUSTAINABILITY
RESEARCH
Open Access

www.advenergysustres.com

1.5 eV GaInAsP Solar Cells Grown via Hydride Vapor-Phase Epitaxy for Low-Cost GaInP/GaInAsP//Si Triple-Junction Structures

Yasushi Shoji,* Ryuji Oshima, Kikuo Makita, Akinori Ubukata, and Takeyoshi Sugaya

Multijunction solar cells combining III–V and Si materials can provide high photoelectric conversion efficiency. Two-terminal III–V//Si triple-junction solar cells with an efficiency of 35.9% have already been developed using metal–organic vapor-phase epitaxy and the direct wafer bonding technique. This study, however, proposes the low-cost fabrication of III–V solar cells using hydride vapor-phase epitaxy (HVPE). GaInAsP solar cells are fabricated using HVPE to apply to middle cells in III–V//Si triple-junction structures. By controlling the partial pressure of the precursors, the optimal bandgap energy of 1.5 eV is obtained for the HVPE-grown GaInAsP quaternary alloys. The 1.5 eV GaInAsP single-junction solar cells show higher open-circuit voltage than the HVPE-grown GaAs solar cells. The open-circuit voltage of the GaInAsP solar cells fabricated with a GaInAsP growth rate of 77.6 µm h^{-1} reaches 1.1 V upon the formation of the rear-heterojunction structure. In addition, the external quantum efficiency spectra of the HVPE-grown GaInP/GaInAsP dual-junction solar cells show that the 1.5 eV GaInAsP solar cells are superior to the GaAs solar cells in terms of current matching for subcells in the III–V//Si triple-junction structures.

1. Introduction

Photovoltaic power generation must be increased toward a sustainable society. However, in some countries or regions, the flat grounds for installing solar panels have already saturated. Furthermore, most of the terrestrial photovoltaics are Si single-junction solar cells with limit efficiencies of ≈30%. Therefore,

Y. Shoji, R. Oshima, K. Makita, T. Sugaya
Global Zero Emission Research Center (GZR)
National Institute of Advanced Industrial Science and Technology (AIST)
1-1-1 Umezono, Tsukuba, Ibaraki 305-8568, Japan
E-mail: y.shoji@aist.go.jp

A. Ubukata
Innovation
Taiyo Nippon Sanso Corporation
10 Okubo, Tsukuba, Ibaraki 300-2611, Japan

The ORCID identification number(s) for the author(s) of this article can be found under https://doi.org/10.1002/aesr.202200198.

the use of multijunction solar cells with a high conversion efficiency needs to be accelerated.[1–3] For III–V solar cells, multijunction technologies, such as tunnel-junction, graded buffers, and semiconductor bonding methods, have been developed to achieve high conversion efficiencies exceeding 30%.[4–9] Nevertheless, they cannot be widely used for terrestrial applications due to their high production cost. In the conventional growth method, i.e., metal–organic vapor-phase epitaxy (MOVPE), expensive organic metals and a high V/III ratio result in high production costs. Therefore, we focused on hydride vapor-phase epitaxy (HVPE) to reduce the epitaxial growth cost of III–V compound materials used in multijunction solar cells.[10–16] In HVPE, inexpensive metal chlorides can be used as group-III precursors via in situ reactions involving pure metals and the HCl gas. Furthermore, high-quality single crystals can be grown at a low V/III ratio, reducing the cost of production.[17–20] With the evolution of HVPE technology, the performance of HVPE-grown solar cells has been improved. In particular, the successful development of Al-containing passivation layers has remarkably enhanced the conversion efficiency,[21,22] achieving 28.3% in GaInP/GaAs dual-junction cells.[23]

The GaAs substrate used for epitaxial growth is another factor that increases the production cost. To reduce the substrate costs, some researchers have attempted direct epitaxial growth of III–V materials on Si substrates.[24–29] However, high-quality III–V materials are difficult to achieve using this method because crystal defects are caused by mismatches of the lattices and thermal expansion coefficients and by antiphase boundaries between III–V and Si. Although these technical challenges have not been completely solved, progress in growth technology has boosted the conversion efficiency of direct-grown GaInP/GaAs/Si triple-junction solar cells to 25.9%.[30] Reuse of GaAs substrates using epitaxial lift-off (ELO) technology has alternatively been proposed for reducing the substrate cost.[31–37] ELO technology separates the solar cells from the substrates. Recently, high-quality Al(Ga)As release layers required for the ELO process have been grown using HVPE, and the ELO of III–V devices fabricated using HVPE has also been demonstrated.[38,39] The ELO technology offers advantages in fabricating multijunction structures. Solar cells peeled from the substrate using ELO technology

can be bonded to other solar cells using metal nanoparticles. This bonding technology is called smart stack,[40] which enables the bonding of semiconductors of dissimilar materials, such as GaAs//Si[41,42] and GaAs//CIGS.[43,44] Using the smart stack technology, we demonstrated 30.8% efficient GaInP/AlGaAs//Si triple-junction solar cells.[45] When Si is used for the bottom cell of a two-terminal triple-junction structure, the optimum bandgap energy of the middle cell is 1.5 eV. AlGaAs and GaInAsP can possess this bandgap energy and can be lattice-matched to the GaAs substrate. Schygulla et al. reported that GaInAsP is more suitable as an absorber for the middle cell and achieved a conversion efficiency of 35.9% for GaInP/GaInAsP//Si triple-junction cells using the direct wafer bonding technique.[46] The III–V semiconductors in their devices were grown using MOVPE. We propose a low-cost fabrication method of GaInP/GaInAsP//Si triple-junction solar cells. The procedure is shown in **Figure 1**. HVPE is used to replace MOVPE for the low-cost fabrication of the GaInP/GaInAsP dual-junction structure. An Al(Ga)As release layer is introduced between the GaAs substrate and cell structure. After growing the III–V cell structure, ELO is performed to separate the solar cell from the substrate. The peeled III–V cells are attached to temporary substrates for handling. The substrate is reusable after separation, which dramatically reduces the production cost. For Si cells, Pd nanoparticles are decorated on the surface to obtain conductivity at the bonding interface with III–V solar cells. After that, GaInP/GaInAsP dual-junction cells and Si single-junction cells are bonded at room temperature. The primary difficulty in this process is to fabricate high-performance GaInAsP solar cells using HVPE. Jain et al. reported 1.7 eV GaInAsP solar cells grown via HVPE.[47] They intended to develop top cells for four-terminal III–V//Si solar cells. Although four-terminal tandem cells do not require current matching between subcells, optical losses such as parasitic absorption and reflectance at

the interface must be minimized to obtain high conversion efficiency. Furthermore, as four-terminal devices require more wirings, the fabrication process of the modules becomes complicated and may itself increase the cost. The fabrication of GaInAsP cells with a bandgap of 1.5 eV via HVPE for application in two-terminal triple-junction structures has never been reported. In this work, we first examined growth conditions for the fabrication of GaInAsP solar cells. Then, we presented the performance of 1.5 eV HVPE-grown GaInAsP single-junction solar cells for the realization of low-cost triple-junction devices.

2. Results and Discussion

2.1. Growth of GaInAsP Layers

First, we investigated the growth conditions to obtain a bandgap energy of 1.5 eV for GaInAsP layers. **Figure 2** shows the peak energy of the photoluminescence (PL) spectrum of GaInAsP layers as a function of the partial pressures of HCl over Ga, HCl (Ga) (Figure 2a), HCl over In, HCl (In) (Figure 2b), and PH_3 (Figure 2c). The PL measurements were conducted at 295 K. The partial pressures of other precursors involved in the growth of GaInAsP layers were kept constant. The PL peak energy of GaInAsP varied with the partial pressure of each precursor, suggesting that the composition of GaInAsP quaternary alloys can be easily controlled by changing the partial pressures of the precursors in case of HVPE. Figure 2d shows the PL spectrum of the GaInAsP grown with partial pressures of HCl(Ga), HCl(In), AsH_3, and PH_3 set to 1.5×10^{-3}, 0.3×10^{-3}, 9.8×10^{-3}, and 4.9×10^{-3} atm, respectively. The peak energy of the PL spectrum was 1.5 eV. An asymmetric spectrum with a high-energy tail specific to band-to-band transition was observed.[48,49] The
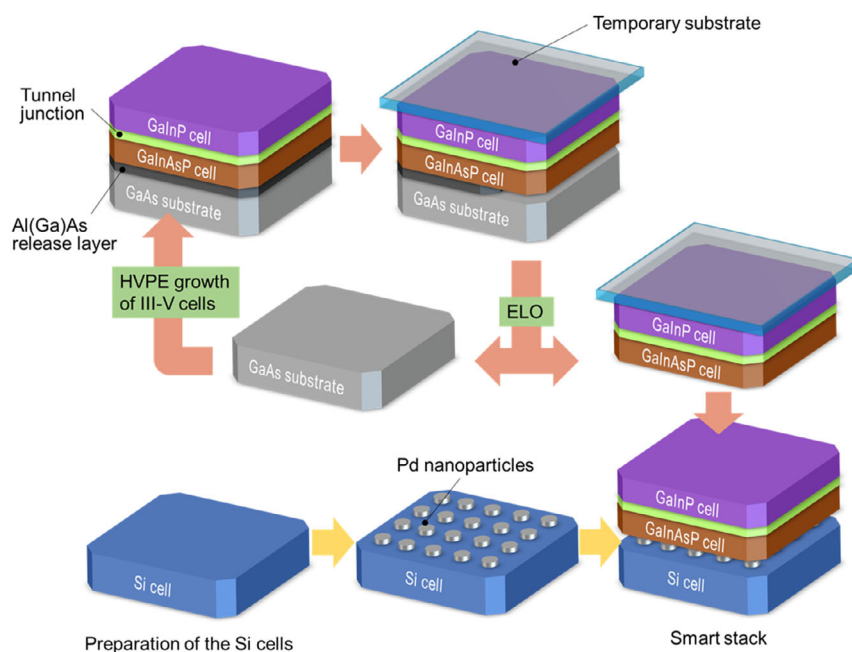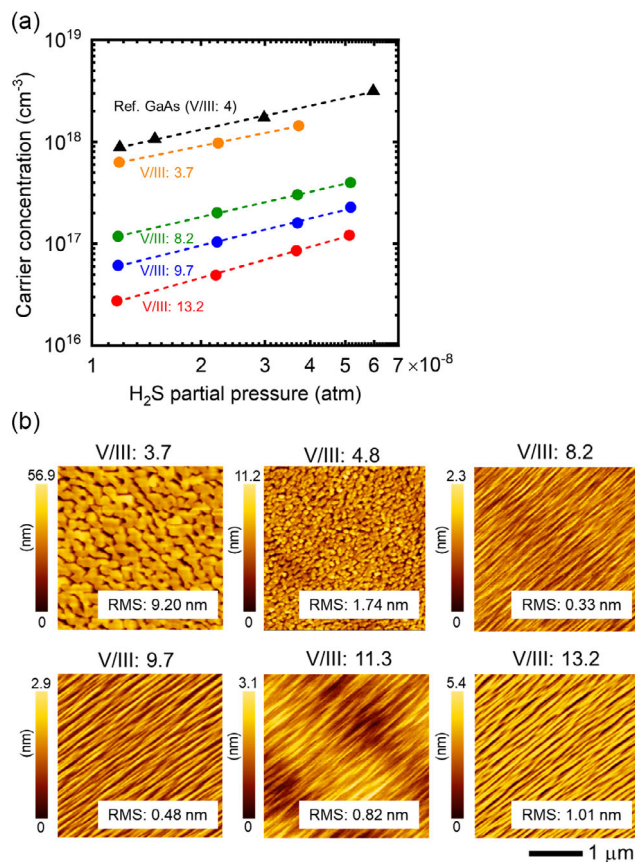

Figure 1. Fabrication procedure for low-cost III–V//Si tandem solar cells.
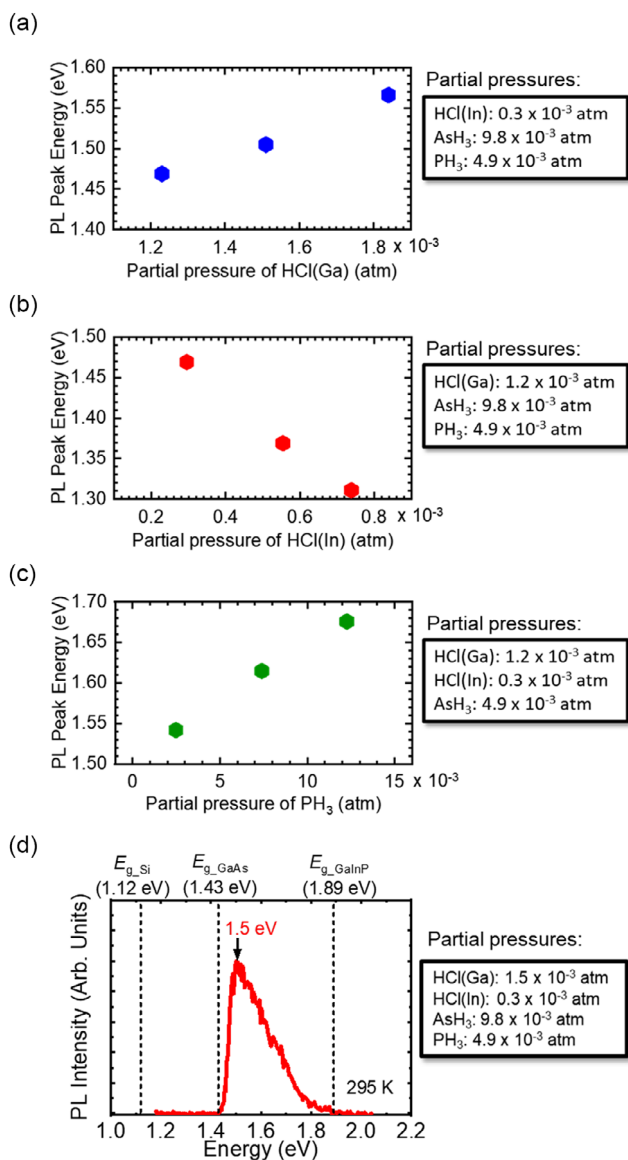
Figure 2. PL peak energy of GaInAsP layers as a function of the partial pressures of a) HCl (Ga), b) HCl (In), and c) PH$_3$. d) PL spectrum of the GaInAsP grown using HCl (Ga), HCl (In), AsH$_3$, and PH$_3$ partial pressures of 1.5×10^{-3}, 0.3×10^{-3}, 9.8×10^{-3}, and 4.9×10^{-3} atm, respectively.

Figure 3. a) Free carrier concentration of S-doped GaInAsP as a function of H$_2$S partial pressure. b) Surface morphology of HVPE-grown GaInAsP obtained using AFM.

spectrum shape reflects the density of states in the electronic structure and the Boltzmann distribution of carriers in GaInAsP alloys.[48,49] Hence, this result indicates that GaInAsP with a 1.5 eV bandgap energy was obtained using HVPE.

Next, we characterized the free carrier concentration of GaInAsP layers to fabricate device structures. **Figure 3**a shows the carrier concentration of S-doped GaInAsP as a function of H$_2$S dopant partial pressure. The GaInAsP layers were adjusted to obtain a bandgap of approximately 1.5 eV and lattice match with the GaAs substrate. The free carrier concentrations were determined via electrochemical capacitance–voltage measurements (ECV). In this study, all S-doped GaInAsP layers showed n-type conductivity, and their carrier concentrations were linearly proportional to the
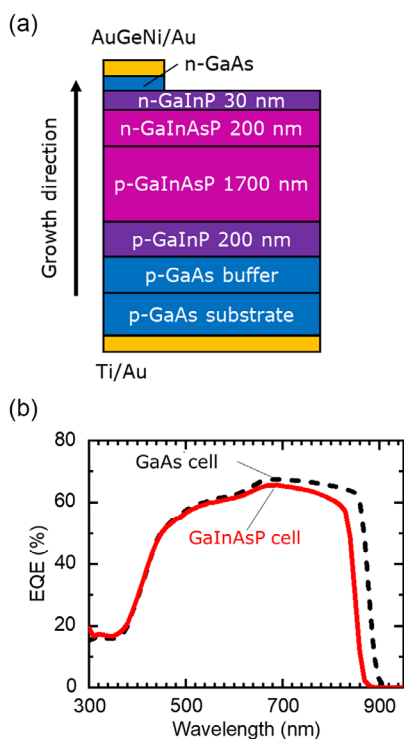
partial pressure of H$_2$S. The slope obtained for GaInAsP layers grown with a V/III ratio of 3.7 is well matched with that of GaAs layers grown with a V/III ratio of 4. As S atoms substitute for the group-V sites, the incorporated S amount increases as the V/III ratio decreases. Then, we characterized the relation between the surface morphology and the V/III ratio of GaInAsP layers.
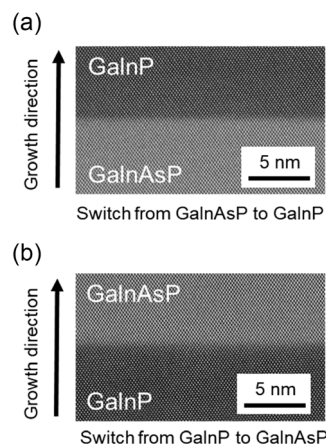
Figure 3b shows the surface morphologies of GaInAsP observed by employing atomic force microscopy (AFM). 3D growth with large unevenness was observed for samples grown with a low V/III ratio (≤ 4.8). We considered that 2D growth did not occur due to the shortage of group-V supply. In contrast, samples grown at a V/III ratio ≥ 8.2 exhibited good surface flatness with atomic steps due to the usage of vicinal substrates. The root-mean-square (RMS) roughness values of the surfaces were found to be in the range of 0.33–1.01 nm. These values are consistent with those of GaAs and GaInP layers grown via HVPE.[16,50] The RMS roughness increased slightly as the V/III ratio increased (>8.2). We believe that this is because the migration length of Ga and In adatoms decreases slightly as the V/III ratio increases. From the viewpoint of surface flatness and carrier concentration, we fabricated GaInAsP cell structures with a V/III ratio of 8.2 in this study. Although the V/III ratio of 8.2 is relatively high for the growth of III–V materials using HVPE, it is substantially smaller than that obtained using MOVPE.[17]

2200198 (3 of 8)

2.2. Characterization of GaInAsP Solar Cells

Figure 4a shows the test structures used to investigate the photo-absorption characteristics of the GaInAsP front-homojunction (FJ) solar cells. The external quantum efficiency (EQE) spectra of the GaInAsP FJ solar cells grown via HVPE are shown in Figure 4b. For comparison, the EQE spectrum of the GaAs FJ cells grown via HVPE is also shown (dashed line). Here, the thickness of the GaAs absorber was 2650 nm for GaAs solar cells. The antireflective coating (ARC) was not applied to GaInAsP and GaAs FJ solar cells, confirming that the light absorption edge of the GaInAsP solar cells had a shorter wavelength than that of the GaAs solar cells. Both samples exhibited almost the same maximum EQE, indicating that the quality of GaInAsP quaternary alloys is comparable to that of GaAs grown via HVPE. The difference in EQE in the long-wavelength region around absorption edges originates from the different absorber thickness. **Figure 5**a,b shows the cross-sectional high-angle annular dark-field scanning transmission electron microscopy (HAADF STEM) images of the GaInP/GaInAsP and GaInAsP/GaInP heterointerfaces, respectively. The former switched to GaInP growth after the growth of the GaInAsP layer, and the latter switched to GaInAsP growth after the growth of the GaInP layer. Although both GaInP and GaInAsP layers were deposited in the same growth chamber, the heterointerfaces exhibited abrupt changes, suggesting good interface quality.

Figure 5. Cross-sectional HAADF STEM images of a) GaInP/GaInAsP and b) GaInAsP/GaInP heterointerfaces.

Next, we investigated the effects of cell structure on the performance of 1.5 eV GaInAsP single-junction cells. Two types of samples with different junction structures were prepared: the FJ structure and the rear-heterojunction (RHJ) structure, as shown in **Figure 6**a. The n-GaInAsP and p-GaInAsP layers were grown at growth rates of 77.6 and 81.5 $\mu m \, h^{-1}$, respectively, for both solar cells. Figure 6b shows the light current–voltage (J–V) curves of both GaInAsP solar cells measured under air mass 1.5 global (AM1.5G) solar spectrum illumination. The performances of the samples without an ARC were compared for an
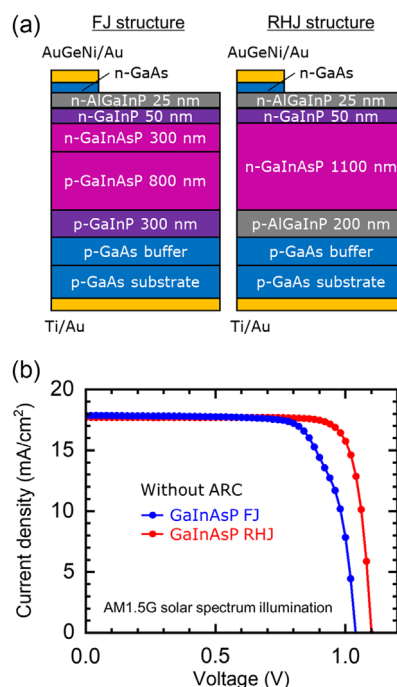

Figure 4. a) Schematic of the test structure used to investigate the photo-absorption characteristics of GaInAsP FJ solar cells. b) EQE spectra of GaInAsP and GaAs single-junction solar cells without an ARC. The solid red and dashed black lines represent the data obtained from GaInAsP and GaAs single-junction solar cells, respectively.

Figure 6. a) Schematic of GaInAsP solar cells with different junction structures. b) Light J–V curves of GaInAsP single-junction solar cells with different structures. The blue and red lines represent the data obtained from FJ and RHJ structures, respectively. An ARC is not employed for these devices.

**ADVANCED
SCIENCE NEWS**

www.advancedsciencenews.com

**ADVANCED
ENERGY & SUSTAINABILITY
RESEARCH**
Open Access

www.advenergysustres.com

impartial evaluation to avoid fluctuations due to the influence of the ARC quality. **Table 1** presents the short-circuit current density (J_{SC}), open-circuit voltage (V_{OC}), fill factor (FF), and conversion efficiency (η) for each solar cell determined from the J–V curves. The V_{OC} of the GaInAsP FJ solar cells was found to be 1.039 V. In our previous work, the V_{OC} of the GaAs FJ solar cells grown via HVPE with a similar growth rate was $\approx$0.95 V.[50] An increase of approximately 90 mV in V_{OC} was observed for the GaInAsP cells compared to the GaAs cells owing to the increased bandgap of the absorber layers. Moreover, V_{OC} was improved by adopting the RHJ structure due to the reduced Shockley–Read–Hall recombination in the depletion region by the formation of the RHJ structure.[51,52] In addition, V_{OC} was improved owing to the higher built-in potential obtained by the higher bandgap of the AlGaInP emitter compared to GaInAsP.[53] Consequently, a high V_{OC} of 1.100 V was obtained for the 1.5 eV GaInAsP RHJ cells.

For FJ devices, most of the photogenerated minority carriers can be collected via the built-in electric field drift process for p–n junctions. In RHJ structures, most of the photogenerated minority carriers in the GaInAsP layer must diffuse over a long distance toward the p–n junction. A thick GaInAsP absorption layer is required to obtain a sufficient amount of photocurrent. Therefore, we examined the dependence of the GaInAsP absorber thickness on the EQE spectra of the RHJ solar cells. **Figure 7** shows the EQE spectra of the GaInAsP RHJ solar cells without an ARC. The EQE in the wavelength region longer than the GaInP absorption edge ($\approx$1.88 eV) is important when utilizing GaInAsP cells in III–V//Si triple-junction structures. The EQE around the GaInAsP absorption edge was enhanced by increasing GaInAsP thickness. For devices with a GaInAsP
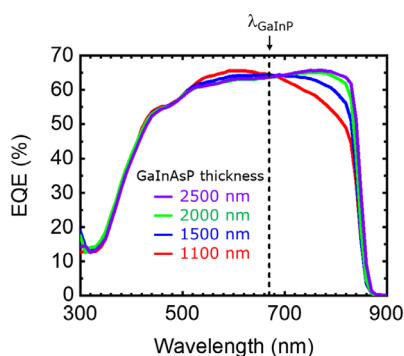
absorption layer having a thickness of $\geq$2000 nm, the shape of the EQE spectra near the absorption edge becomes close to a rectangle, suggesting that photogenerated minority carriers in the GaInAsP absorption layer are sufficiently collected by diffusion even in case of the RHJ structures.

Finally, we characterized the photocurrent of the GaInP/GaInAsP dual-junction structures for bonding with Si cells. **Figure 8** shows the EQE spectra of the GaInP/GaInAsP dual-junction cells. The purple and red curves indicate the EQE spectra of the GaInP top cell and GaInAsP bottom cell, respectively. The GaInAsP cell adopted the RHJ structure, and the thickness of the GaInAsP absorber was set to 2000 nm in this study. For comparison, the EQE spectrum of the GaAs bottom cell in the GaInP/GaAs dual-junction structure is shown by the dashed black line in Figure 8. As for the single-junction structure, the light absorption edge of the GaInAsP bottom cell shifted to a shorter wavelength compared to that of the GaAs cell. The integral values of the EQE spectrum under AM1.5G solar spectrum illumination were 8.1 and 9.8 mA cm^{-2} for the GaInAsP and GaAs subcells, respectively, showing that the two-terminal GaInP/GaInAsP//Si triple-junction structures can increase the Si subcell photocurrent production by approximately 1.7 mA cm^{-2} compared to the GaInP/GaAs//Si triple-junction structure. From the viewpoint of the bandgaps of the constituent materials, in the latter structure, the photocurrent production of the Si bottom cell limits the total photocurrent of the devices.[54] Therefore, it is effective to use 1.5 eV GaInAsP for middle cells in III–V//Si triple-junction structures. We have previously demonstrated the ELO and smart stack processes of HVPE-grown cells.[38,39,55] Further research on smart-stacked HVPE-grown GaInP/GaInAsP dual-junction cells and Si single-junction cells may realize low-cost high-efficiency triple-junction solar cells.

3. Conclusion

We studied 1.5 eV GaInAsP single-junction solar cells grown via HVPE. The bandgap energy of GaInAsP alloys can be controlled by changing the partial pressures of the precursors. The cross-sectional STEM images confirmed that abrupt interfaces can be obtained even if GaInAsP and GaInP were grown in the same growth chamber. The GaInAsP single-junction solar cells

Table 1. Parameters of light J–V curves of GaInAsP single-junction solar cells with different junction structures. An ARC is not employed for these devices.

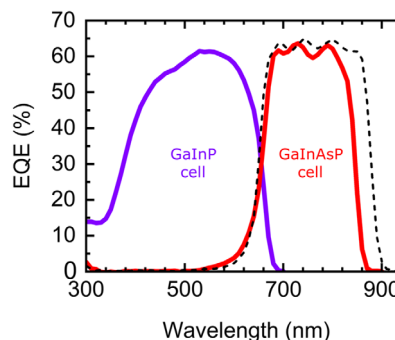| Structure	FJ	RHJ
J_{SC} [mA cm^{-2}]	17.9	17.7
V_{OC} [V]	1.039	1.100
FF [%]	75.2	83.2
η [%]	13.9	16.2

Figure 7. EQE spectra of GaInAsP single-junction cells with different GaInAsP absorption layer thicknesses. The arrow indicates the absorption edge of GaInP solar cells (1.88 eV).

Figure 8. EQE spectra of GaInP/GaInAsP dual-junction cells without an ARC. The solid purple and red lines represent the EQE obtained from the GaInP and GaInAsP subcells, respectively. The dashed black line is the EQE of the GaAs subcell in GaInP/GaAs dual-junction cells.
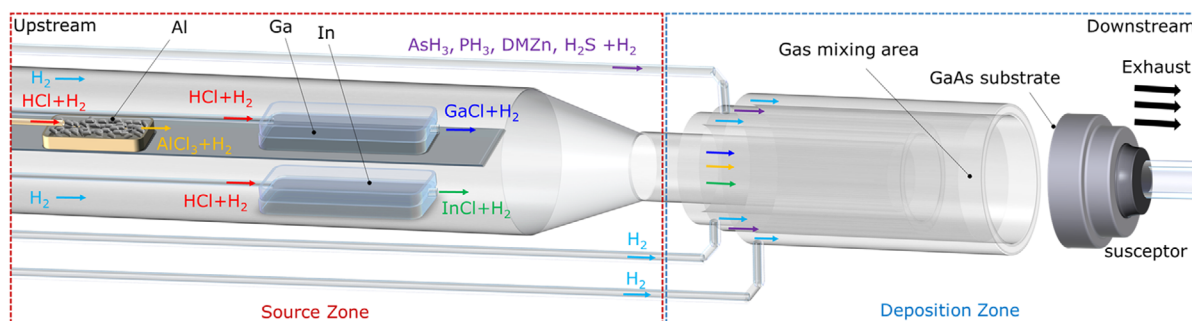
Figure 9. Schematic of the HVPE growth chamber used for the deposition of GaInAsP, GaInP, and AlGaInP layers.

Table 2. Growth rates of materials used in the fabrication of GaInAsP solar cells via HVPE.

Materials	Polarity	Growth rate [$\mu m\,h^{-1}$]
GaAs	n	18.6
	p	19.3
GaInP	n	13.3
	p	32.0
AlGaInP	n	7.4
	p	9.6
GaInAsP	n	77.6
	p	81.5

showed higher V_{OC} than the HVPE-grown GaAs solar cells previously reported by our group. Furthermore, the formation of the RHJ structure improved the cell performance. In particular, V_{OC} was greatly increased from 1.039 to 1.100 V. For the GaInAsP RHJ cells, GaInAsP layers were grown at 77.6 $\mu m\,h^{-1}$, which is much higher than that of typical MOVPE. Compared to the GaAs solar cells, the 1.5 eV GaInAsP solar cells are superior in terms of current matching for subcells in fabricating triple-junction solar cells with Si as the bottom cells. The photocurrent density of the Si bottom cells can be increased by ≈2 mA cm^{-2} in two-terminal GaInP/GaInAsP//Si triple-junction structures compared to that in two-terminal GaInP/GaAs//Si triple-junction structures. Our work demonstrates that high-performance 1.5 eV GaInAsP solar cells can be obtained using low-cost HVPE for the first time. The results represent major progress toward realizing low-cost III–V//Si triple-junction solar cells.

4. Experimental Section

Samples were grown on a GaAs (100) substrate that was miscut 4° toward the (111)B direction. A triple-chamber HVPE system (Taiyo Nippon Sanso, H260) that comprised two growth chambers and a preparation chamber was used for epitaxial growth.[15,21] One growth chamber was used for the deposition of GaAs layers. The other growth chamber was used for the deposition of GaInAsP, GaInP, and AlGaInP layers. **Figure 9** shows a schematic of the latter. The source zone used for the preparation of metal chlorides was located at the upstream side of the reactor. In the upper part of the source zone, a Ga-filled quartz boat and an Al-filled alumina boat were installed, whereas an In-filled quartz boat was installed in the lower

part. The Ga- and In-filled quartz boats were heated to 700 °C, and HCl gas was introduced to produce GaCl and InCl precursors, respectively. The Al-filled alumina boat was heated to <500 °C, and HCl gas was introduced to generate AlCl$_3$ precursors.[38,56,57] In the growth chambers, 200 ppm H$_2$S and 1000 ppm dimethylzinc in a H$_2$ mixture were supplied as n- and p-type dopant gases, respectively. All gases were transported to the deposition zone by the H$_2$ carrier gas in the reactor. The preparation chamber that maintained a substrate under the flow of group-V precursors of AsH$_3$ or PH$_3$ was located between the two growth chambers. The purpose of this chamber was to stabilize the feed gas when switching gas species or flow rates in the growth chambers. For stabilizing the feed gas, the growth of the samples was paused at all interfaces with implementation times of approximately 1–1.5 min. The substrate attached to the susceptor was moved between the preparation chamber and each growth chamber within ≈2 s. During sample growth, the temperature of the deposition zone was set to 660 °C.

The GaInP and AlGaInP layers were grown such that their lattice is similar to that of GaAs. The growth conditions and compositions are described in previous reports.[21,23] The growth rates of constituent layers for GaInAsP solar cells are summarized in **Table 2**. Ga, In, As, and P compositions in GaInAsP absorbers in the cell structures were ≈95%, ≈5%, ≈89%, and ≈11%, respectively. For the cell structures, AuGeNi/Au and Ti/Au electrodes were deposited as top and bottom contacts, respectively. The GaAs front contact layer was etched using a citric acid solution. Mesa isolation was performed using photolithography for all devices.

The structural properties of the samples were characterized via AFM and STEM. The PL spectra of the GaInAsP layers were obtained using a compact near-infrared PL spectrometer (Hamamatsu, C12132). The wavelength of the excitation laser was 532 nm. The performance of the cells was evaluated through J–V curves using a solar simulator with xenon and halogen dual light sources (Bunkoukeiki), which closely simulate the AM1.5G solar spectrum. Further, EQE spectra were measured using a monochromatic light with a flux of 1×10^{14} photons cm^{-2} (Bunkoukeiki, CEP-25Cl). The signal was detected in the alternating current mode at a chopping frequency of 85 Hz using a lock-in amplifier.

Conflict of Interest

The authors declare no conflict of interest.

Data Availability Statement

Research data are not shared.

[1] C. L. Stender, J. Adams, V. Elarde, T. Major, H. Miyamoto, M. Osowski, N. Pan, R. Tatavarti, F. Tuminello, A. Wibowo, C. Youtsey, G. Ragunathan, in *Proc. 42nd IEEE Photovoltaic Spec. Conf.*, IEEE, Piscataway, NJ **2015**.

[2] M. Yamaguchi, T. Masuda, K. Araki, D. Sato, K. H. Lee, N. Kojima, T. Takamoto, K. Okumura, A. Satou, K. Yamada, T. Nakado, Y. Zushi, Y. Ohshita, M. Yamazaki, *Prog. Photovoltaics Res. Appl.* **2021**, *29*, 684.

[3] T. Masuda, K. Araki, K. Okumura, S. Urabe, Y. Kudo, K. Kimura, T. Nakado, A. Sato, M. Yamaguchi, *Sol. Energy* **2017**, *146*, 523.

[4] R. M. France, J. F. Geisz, T. Song, W. Olavarria, M. Young, A. Kibbler, M. A. Steiner, *Joule* **2022**, *6*, 1121.

[5] J. F. Geisz, R. M. France, S. L. Kevin, M. A. Steiner, A. G. Andrew, H. L. Guthrey, M. R. Young, T. Song, T. Moriarty, *Nat. Energy* **2020**, *5*, 326.

[6] F. Dimroth, T. N. D. Tibbits, M. Niemeyer, F. Predan, P. Beutel, C. Karcher, E. Oliva, G. Siefer, D. Lackner, P. Fus-Kailuweit, A. W. Bett, R. Krause, C. Drazek, E. Guiot, J. Wasselin, A. Tauzin, T. Signamarcheix, *IEEE J. Photovoltaics* **2016**, *6*, 343.

[7] K. Sasaki, T. Agui, K. Nakaido, N. Takahashi, R. Onitsuka, T. Takamoto, *AIP Conf. Proc.* **2013**, *1556*, 22.

[8] P. T. Chiu, D. C. Law, R. L. Woo, S. B. Singer, D. Bhusari, W. D. Hong, A. Zakaria, J. Boisvert, S. Mesropian, R. R. King, N. H. Karam, in *Proc. 40th IEEE Photovoltaic Spec. Conf.*, IEEE, Piscataway, NJ **2014**, p. 11.

[9] M. Yamaguchi, F. Dimroth, J. F. Geisz, N. J. Ekins-Daukes, *J. Appl. Phys.* **2021**, *129*, 240901.

[10] W. D. Johnston Jr., W. M. Callahan, *Appl. Phys. Lett.* **1976**, *28*, 150.

[11] G. H. Olsen, M. Ettenberg, R. V. D'Aiello, *Appl. Phys. Lett.* **1978**, *33*, 606.

[12] J. C. C. Fan, C. O. Bozler, R. L. Chapman, *Appl. Phys. Lett.* **1978**, *32*, 390.

[13] J. Simon, K. L. Schulte, D. L. Young, N. M. Haegel, A. J. Ptak, *IEEE J. Photovoltaics* **2016**, *6*, 191.

[14] K. L. Schulte, J. Simon, J. Mangum, C. E. Packard, B. P. Gorman, N. Jain, A. J. Ptak, *IEEE J. Photovoltaics* **2017**, *7*, 1153.

[15] R. Oshima, K. Makita, A. Ubukata, T. Sugaya, *Jpn. J. Appl. Phys.* **2018**, *57*, 08RD06.

[16] Y. Shoji, R. Oshima, K. Makita, A. Ubukata, T. Sugaya, *Appl. Phys. Express* **2019**, *12*, 052004.

[17] K. L. Schulte, J. Simon, A. Roy, R. C. Reedy, D. L. Young, T. F. Kuech, A. J. Ptak, *J. Cryst. Growth* **2016**, *434*, 138.

[18] A. L. Greenaway, J. W. Boucher, S. Z. Oener, C. J. Funch, S. W. Boettcher, *ACS Energy Lett.* **2017**, *2*, 2270.

[19] J. Simon, K. L. Schulte, K. A. W. Horowitz, T. Remo, D. L. Young, A. J. Ptak, *Crystals* **2019**, *9*, 3.

[20] V. Raj, T. Haggren, W. W. Wong, H. H. Tan, C. Jagadish, *J. Phys. D: Appl. Phys.* **2022**, *55*, 143002.

[21] Y. Shoji, R. Oshima, K. Makita, A. Ubukata, T. Sugaya, *Prog. Photovoltaics Res. Appl.* **2021**, *29*, 1285.

[22] J. T. Boyer, K. L. Schulte, M. R. Young, A. J. Ptak, J. Simon, *Prog. Photovoltaics Res. Appl.* **2023**, *31*, 230.

[23] Y. Shoji, R. Oshima, K. Makita, A. Ubukata, T. Sugaya, *Sol. RRL* **2022**, *6*, 2100948.

[24] M. Yamaguchi, C. Amano, Y. Itoh, *J. Appl. Phys.* **1989**, *66*, 915.

[25] T. Soga, T. Kato, M. Yang, M. Umeno, T. Jimbo, *J. Appl. Phys.* **1995**, *78*, 4196.

[26] M. Yamaguchi, Y. Ohmachi, T. Oh'hara, Y. Kadota, M. Imaizumi, S. Matsuda, *Prog. Photovoltaics Res Appl.* **2001**, *9*, 191.

[27] K. N. Yaung, M. Vaisman, J. Lang, M. L. Lee, *Appl. Phys. Lett.* **2016**, *109*, 032107.

[28] T. J. Grassman, D. J. Chmielewski, S. D. Carnevale, J. A. Carlin, S. A. Ringel, *IEEE J. Photovoltaics* **2016**, *6*, 326.

[29] M. Feifel, D. Lackner, J. Ohlmann, J. Benick, M. Hermle, F. Dimroth, *Sol. RRL* **2019**, *3*, 1900313.

[30] M. Feifel, D. Lackner, J. Schön, J. Ohlmann, J. Benick, G. Siefer, F. Predan, M. Hermle, F. Dimroth, *Sol. RRL* **2021**, *5*, 2000763.

[31] M. Konagai, M. Sugimoto, K. Takahashi, *J. Cryst. Growth* **1978**, *45*, 277.

[32] E. Yablonovitch, T. Gmitter, J. P. Harbison, R. Bhat, *Appl. Phys. Lett.* **1981**, *51*, 2222.

[33] J. J. Schermer, P. Mulder, G. J. Bauhuis, P. K. Larsen, G. Oomen, E. Bongers, *Prog. Photovoltaics Res. Appl.* **2005**, *13*, 587.

[34] G. J. Bauhuis, P. Mulder, E. J. Haverkamp, J. J. Schermer, E. Bongers, G. Oomen, W. Köstler, G. Strobl, *Prog. Photovoltaics Res. Appl.* **2010**, *18*, 155.

[35] W. Choi, C. Z. Kim, C. S. Kim, W. Heo, T. Joo, S. Y. Ryu, H. Kim, H. Kim, H. K. Kang, S. Jo, *Adv. Energy Mater.* **2014**, *4*, 1400589.

[36] S. Moon, K. Kim, Y. Kim, J. Heo, J. Lee, *Sci. Rep.* **2016**, *6*, 30107.

[37] A. P. Kirk, D. W. Cardwell, J. D. Wood, A. Wibowo, K. Forghani, D. Rowell, N. Pan, M. Osowski, in *Proc. 7th World Conf. on Photovoltaic Energy Conversion (WCPEC) (A Joint Conf. of 45th IEEE PVSC, 28th PVSEC & 34th EU PVSEC)*, IEEE, Piscataway, NJ **2018**, p. 0032.

[38] Y. Shoji, R. Oshima, K. Makita, A. Ubukata, T. Sugaya, *IEEE J. Photovoltaics* **2021**, *11*, 93.

[39] Y. Shoji, R. Oshima, K. Makita, A. Ubukata, T. Sugaya, *Sol. Energy* **2021**, *224*, 142.

[40] H. Mizuno, K. Makita, K. Matsubara, *Appl. Phys. Lett.* **2012**, *101*, 191111.

[41] H. Mizuno, K. Makita, T. Mochizuki, T. Tayagaki, T. Sugaya, H. Takato, *ACS Appl. Energy Mater.* **2020**, *3*, 3445.

[42] H. Mizuno, K. Makita, H. Sai, T. Mochizuki, T. Matsui, H. Takato, R. Müller, D. Lackner, F. Dimroth, T. Sugaya, *ACS Appl. Energy Mater.* **2022**, *14*, 11322.

[43] K. Makita, Y. Kamikawa, H. Mizuno, R. Oshima, Y. Shoji, S. Ishizuka, R. Müller, P. Beutel, D. Lackner, J. Benick, M. Hermle, F. Dimroth, T. Sugaya, *Prog. Photovoltaics Res. Appl.* **2021**, *29*, 887.

[44] K. Makita, Y. Kamikawa, T. Koida, H. Mizuno, R. Oshima, Y. Shoji, S. Ishizuka, T. Takamoto, T. Sugaya, *Prog. Photovoltaics Res. Appl.* **2023**, *31*, 71.

[45] K. Makita, H. Mizuno, T. Tayagaki, T. Aihara, R. Oshima, Y. Shoji, H. Sai, H. Takato, R. Müller, P. Beutel, D. Lackner, J. Benick, M. Hermle, F. Dimroth, T. Sugaya, *Prog. Photovoltaics Res. Appl.* **2020**, *28*, 16.

[46] P. Schygulla, R. Müller, D. Lackner, O. Höhn, H. Hauser, B. Bläsi, F. Predan, J. Benick, M. Hermle, S. W. Glunz, F. Dimroth, *Prog. Photovoltaics Res. Appl.* **2022**, *30*, 869.

[47] N. Jain, J. Simon, K. L. Schulte, D. J. Friedman, D. R. Diercks, C. E. Packard, D. L. Young, A. J. Ptak, *IEEE J. Photovoltaics* **2018**, *6*, 1577.

[48] Z. C. Su, S. J. Xu, R. X. Wang, J. Q. Ning, J. R. Dong, S. L. Lud, H. Yang, *Sol. Energy Mater. Sol. Cells* **2017**, *168*, 201.

[49] X. Li, J. Xu, T. Wei, W. Yang, S. Jin, Y. Wu, S. Lu, *Crystals* **2021**, *11* 1590.

[50] R. Oshima, Y. Shoji, K. Makita, A. Ubukata, T. Sugaya, *J. Cryst. Growth* **2020**, *537*, 125600.

[51] J. F. Geisz, M. A. Steiner, I. García, S. R. Kurtz, D. J. Friedman, *Appl. Phys. Lett.* **2013**, *103*, 041118.

[52] D. L. Lepkowski, J. T. Boyer, D. J. Chmielewski, A. C. Silvaggio, S. A. Ringel, T. J. Grassman, *IEEE J. Photovoltaics* **2019**, *9*, 1644.

[53] S. T. Hwang, S. Kim, H. Cheun, H. Lee, B. Lee, T. Hwang, S. Lee, W. Yoon, H. M. Lee, B. Park, *Sol. Energy Mater. Sol. Cells* **2017**, *155*, 264.

[54] K. Derendorf, S. Essig, E. Oliva, V. Klinger, T. Roesener, S. P. Philipps, J. Benick, M. Hermle, M. Schachtner, G. Siefer, W. Jager, F. Dimroth, *IEEE J. Photovoltaics* **2013**, *3*, 1423.

[55] Y. Shoji, H. Sai, R. Oshima, K. Makita, T. Matsui, A. Ubukata, T. Sugaya, in *8th World Conf. on Photovoltaic Energy Conversion (WCPEC-8)* **2022**, p. 2AV.3.25.

[56] A. Koukitu, F. Satoh, T. Yamane, H. Murakami, Y. Kumagai, *J. Cryst. Growth* **2005**, *281*, 47.

[57] K. L. Schulte, W. Metaferia, J. Simon, D. Guiling, K. Udwary, G. Dodson, J. H. Leach, A. J. Ptak, *ACS Appl. Energy Mater.* **2019**, *2*, 8405.